

Lupsix: A Cascade Framework for Lung Parenchyma Segmentation in Axial CT Images

Hasan Koyuncu*¹

Accepted : 31/12/2018 Published: 31/12/2018

Abstract: Lung imaging and computer aided diagnosis (CAD) play a critical role in detection of lung diseases. The most significant part of a lung based CAD is to fulfil the parenchyma segmentation, since disease information is kept in the parenchyma texture. For this purpose, parenchyma segmentation should be accurately performed to find the necessary diagnosis to be used in the treatment. Besides, lung parenchyma segmentation remains as a challenging task in computed tomography (CT) owing to the handicaps oriented with the imaging and nature of parenchyma. In this paper, a cascade framework involving histogram analysis, morphological operations, mean shift segmentation (MSS) and region growing (RG) is proposed to perform an accurate segmentation in thorax CT images. In training data, 20 axial CT images are utilized to define the optimum parameter values, and 150 images are considered as test data to objectively evaluate the performance of system. Five statistical metrics are handled to carry out the performance assessment, and a literature comparison is realized with the state-of-the-art techniques. As a result, parenchyma tissues are segmented with success rates as 98.07% (sensitivity), 99.72% (specificity), 99.3% (accuracy), 98.59% (Dice similarity coefficient) and 97.23% (Jaccard) on test dataset.

Keywords: Axial Analysis, Computed Tomography, Cascade Framework, Lung Parenchyma, Medical Image Segmentation

1. Introduction

Lung segmentation reserves a significant place before important objectives like detection of pulmonary nodules, pulmonary vessels, cancer types and various diseases [1-4]. In medical area, computed tomography (CT) scans are frequently preferred to perform a diagnostic about aforementioned subjects. Herein, thorax CT images constitute some challenging handicaps for an accurate parenchyma segmentation. These handicaps arise as: 1-) Similar grey levels between the lung parenchyma and other tissues, 2-) Disease based deformation inside of parenchyma, 3-) Non-stable shape features of lung tissues. For this purpose, various segmentation algorithms are asserted in the literature: Thresholding approaches, Region-based algorithms, Shape-based methods, Neighboring anatomy-guided techniques and Machine learning-based structures [5-7].

Thresholding approaches work efficient, once lung intensities clearly differentiate from the close tissues. However, these techniques cannot be used on conditions that spatial information and variability gain importance related to the disease based deformations. At this point, deformations can sharply change the grey values in lung [5]. Region-based algorithms (region growing, fuzzy connectedness, graph cut, etc.) are seen as impressive techniques containing spatial information with region phenomena. Region-based methods are actively utilized on homogenous-field in lung, but the performance of techniques vary on the segmentation of heterogeneous fields [5]. Shape-based methods (atlas or model – based methods, active contours, level sets, etc.) are frequently appealed to segment the abnormal tissues on which thresholding approaches remain insufficient [5]. Neighboring anatomy-guided techniques consider neighboring anatomic objects

around lung for separating the lung from objects (organs). Nevertheless, these techniques cannot be processed on extremely abnormal or artifacted lung parenchyma [5]. Similarly, performance of machine learning-based methods can deteriorate sharply because of the extreme deformation inside of lung parenchyma [5]. In the literature, aforementioned techniques have been applied to the lung segmentation, and hybrid techniques are being designed to handle the parenchyma segmentation with higher performance [5-8].

Wei et al. [9] developed a system based on improved chain code and Bresenham algorithm to segment the lungs. Proposed system performed the task with an accuracy of 95.2%. Dai et al. [10] designed a pipeline involving graph cuts, Gaussian mixture models (GMMs) and expectation maximization (EM) to segment the lungs. According to the results, proposed model obtained the Dice similarity coefficient (DSC) as 98.74%. Noor et al. [11] realized lung segmentation with a framework in which thresholding and morphology based process are used. In experiments, it was revealed that proposed method performed the segmentation with high DSC (98.4%). Pulagam et al. [12] utilized the modified convex hull approach and morphological operators for segmentation. According to the experiments, proposed approach obtained 98.62% DSC on overall. Chae et al. [13] generated a Level-set based approach named MLevel-set that achieved 98.4% accuracy on lung segmentation. Zhang et al. [14] produced a hybrid geometric active contour model and attained with 97.7% DSC on average.

In this paper, a cascade framework is presented to segment the parenchyma tissue in CT images as more proper than the state-of-the-art methods. Histogram analysis, morphological operations, mean shift segmentation (MSS) and region growing (RG) are handled to design an efficient framework. Proposed system is named according to the tasks to be realized including the number of units (six): Lupsix (**l**ung **p**arenchyma **s**egmentation **i**n **a**xial **C**T).

¹ Konya Technical University, Konya, TURKEY

* Corresponding Author: Email: hasankoyuncu@selcuk.edu.tr

Performance of Lupsix is evaluated in CT images taken from LUNA16 dataset, with the use of five different metrics [15-17]. The rest of paper is organized as follows. In Section 2, the utilized methods and Lupsix are comprehensively explained. In Section 3, performance evaluation is examined in detail, and visual perspectives of results are presented to qualify the operation of system. The interpretations of work are mentioned, and a literature comparison is tendered. In Section 4, concluding remark is given.

2. Methods

The principle of this study is to obtain the lungs in thorax-axial CT images in which shape features of lungs varies uncharacteristically, diseases based deformation can be available and lung parenchyma can own to close grey levels with the nearby tissues. This situation requires a robust framework that will not effected from these handicaps, and the following methods are utilized to design a robust system:

- Gamma correction
- Morphological closing
- Contrast-limited adaptive histogram equalization
- Mean shift segmentation
- Region growing
- The filling process

2.1. Morphological Algorithms

Gamma correction: Gamma correction (GC) stands for a contrast enhancement method explicitly revealing the objects in image. GC is generally utilized to improve the nonlinearity of image and regarding this, the intensities are rearranged as in (1) [18].

$$v_{out} = (A \cdot v_{input})^\gamma \quad (1)$$

v_{input} , A and γ respectively symbolize the input image, constant and the power. Mapping process of gamma correction constitutes a linear transformation in the event that A and γ are equal to "1", and pixel intensities are settled within the range [0,1] as in our study [18].

Morphological closing: Morphological closing (MC) is used to combine the familiar pixel intensities according to the structuring element (diamond, disk, line, etc.). For this purpose, *closing* process ($A \bullet B$) is formed as in (2) of which $A \oplus B$ and θB respectively symbolize the *dilation* of A and B , and *erosion* of B [19].

$$A \bullet B = (A \oplus B) \theta B \quad (2)$$

As a result of MC, the objects in an image come to the forefront better than the initial conditions. Hence, MC can be efficiently preferred on object detection and segmentation tasks [19,20].

Contrast - limited adaptive histogram equalization: Contrast-limited adaptive histogram equalization (CLAHE) varies from the adaptive histogram equalization (AHE) with the use of *contrast limiting* (CL). Herein, AHE is a transformation of pixels concerning the *histogram* and *neighboring* so as to improve the irregular contrast distribution. CL represses the increase in noise level arisen as a result of contrast level increase [21].

Filling process: The filling process is used to fill the areas connected with each other, and these areas consist of closed shapes to be filled [22].

2.2. Mean Shift Segmentation

Mean shift segmentation (MSS) defines the 2D features of an image into the joint spatial-range domain. In operation of MSS, mode values are considered to rearrange the pixels' intensities of different clusters. Two kernels are analyzed to attach the pixels of an object: 1-) Spatial kernel, 2-) Range kernel. The bandwidths of kernels play a critical role for the optimum attachment of pixels of the same cluster (object). MSS algorithm includes three parameters to approximate the pixels [23]:

- Spatial kernel bandwidth (h_s)
- Range kernel bandwidth (h_r)
- Convergence criterion threshold (M)

To attach the pixels, MSS operates a multiple-kernel stated in (3) [23,24].

$$K_{h_s, h_r}(x) = \frac{C}{h_s^2 h_r^p} k\left(\left\|\frac{x^s}{h_s}\right\|^2\right) k\left(\left\|\frac{x^r}{h_r}\right\|^2\right) \quad (3)$$

x^s and x^r symbolize the vectors concerning with the spatial and range phenomena; $k(x)$, C and p respectively mean the general profile, normalization coefficient and dimension. Herein, the spatial (h_s) and range (h_r) kernel bandwidths should be carefully assigned to optimally detect the objects. Besides, the pixels owing to lower grey values than threshold M , are ignored to perform the specified-size segmentation. For a detailed explanation about MSS, please see [23] and [24].

2.3. Region Growing

Region growing (RG) starts with a random or user-defined point (seed) in image. According to seed intensity, the extension of pixels continue until similar intensities are not available. For this purpose, a parameter is needed to decide which pixel value will be included or excluded. This parameter (*tolerance*) is regarded to restrict the extension of pixels. RG algorithm processes step by step according to the following rules [24]:

- Assignment of seed point(s)
- The extension is realized which is restricted by *tolerance*
- The extension is performed according to neighbor pixel intensities until termination is met

2.4. Lupsix Framework

In Lupsix; histogram analysis, morphological operators, MSS and RG algorithms are chosen to reveal the parenchyma tissue, and to design a robust system against aforementioned handicaps. For this purpose, Lupsix runs the operation steps in Figure 1:

1. GC differentiates the regions inside of thorax CT image. At this point, lung parenchyma differs from the nearby tissues like ribs, subcutaneous fats, etc.
2. MC is performed with *disk* type structuring element, since this type element remains as the most proper one in terms of fitting to the concavity of lungs. After MC is processed, the parenchyma intensities come to closer grey levels for an accurate object segmentation.
3. CLAHE sharpens the outer edges of parenchyma. However, this situation puts forward more sensitive changes inside of parenchyma, and some parts of lung (like nodules, vessels, etc.) are sharpened too.
4. MSS attaches the tissue parts of parenchyma to reveal and to smooth the parenchyma more explicit. Regarding this, thorax CT image becomes more convenient before object segmentation.
5. RG is fulfilled using two user-defined seed points, and lung parenchyma is segmented with the use of MSS

output (image containing smoothed and attached objects).

6. The filling process is realized to combine the small gaps comprising of circumscribed areas within the parenchyma tissues.
7. System output is obtained by multiplying the output of filling process (binary mask) with the output of GC.

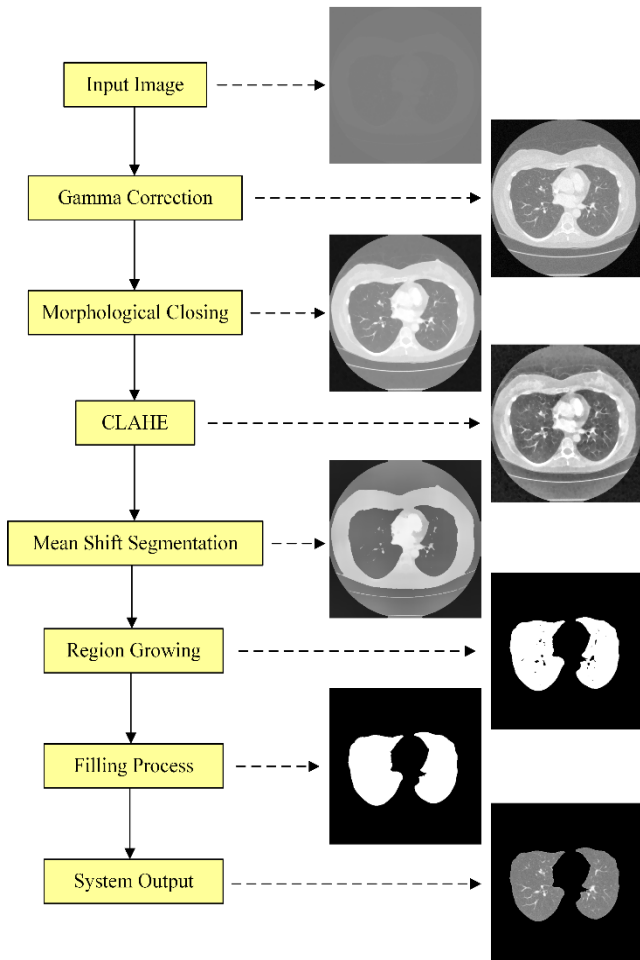


Fig. 1. Flowchart of proposed framework

In Lupsix, five parameters should be examined in detail to perform an accurate segmentation:

- *Tolerance* in RG
- *Size of structuring element* in MC
- *Spatial kernel bandwidth* (h_s)
- *Range kernel bandwidth* (h_r)
- *Threshold* in MSS (M)

3. Results and Discussions

In this section; parameter adjustment, training & test results, visual results, interpretations and literature comparison are presented in a comprehensive and brief manner. All experiments were performed in Matlab software on a personal computer with 2.80 GHz CPU, 16 GB RAM and GeForce GTX 1050Ti graphic card. Performance of framework is evaluated on 170 CT images taken from LUNA16 database [15-17]. Five statistical metrics (sensitivity, specificity, accuracy, DSC, Jaccard) are considered to evaluate the performance of system:

$$Sensitivity = TP / (TP + FN) \quad (4)$$

$$Specificity = TN / (TN + FP) \quad (5)$$

$$Accuracy = (TP + TN) / (TP + TN + FP + FN) \quad (6)$$

$$DSC = (2 * TP) / ((2 * TP) + FP + FN) \quad (7)$$

$$Jaccard = TP / (FN + FP + TP) \quad (8)$$

These metrics are preferred according to their efficiency for evaluation of segmentation performance [24, 25]. TP, TN, FP, and FN respectively specify the true positive, true negative, false positive and false negative results among trials [20,24,25].

3.1. Parameter Settings of Lupsix

There exist three rules for design of a robust framework: 1) Formation of units step by step according to the needs, 2) Examination of parameters in detail by using the train data, 3) Detection of the optimum values by using the satisfactory results specified with a tolerance [25]. To actualize this, parameter values stated in Table 1 are handled for an in-depth analysis.

Table 1. Parameter adjustments of Lupsix

| Parameter | Examination Values and Ranges |
|-----------------------------|--|
| Tolerance | 10, 20, 30, 40, 50, 60 |
| Size of structuring element | 2, 3, 4, 5, 6 |
| $[h_s, h_r]$ | [8,8], [16,16], [24,24], [32,32], [40,40], [48,48], [16,8], [16,24], [16,32], [16,40], [16,48], [24,8], [24,16], [24,32], [24,40], [24,48], [32,8], [32,16], [32,24], [32,40], [32,48], [40,8], [40,16], [40,24], [40,32], [40,48], [48,8], [48,16], [48,24], [48,32], [48,40] |
| M | 0.1, 0.2, 0.3, 0.4, 0.5, 0.6, 0.7, 0.8, 0.9, 1, 1.5, 2 |

The bandwidths of spatial (h_s) and feature (h_r) kernels are examined as dual and fold of "4" [13, 24]. Performance of Lupsix sharply deteriorates once tolerance, size of structuring element and M are selected bigger than 60, 6 and 2, respectively. Also different values and conditions stated in Table 1, have been handled, but the results of these trials were unsuitable to present. In brief, Table 1 presents the reliable adjustments having meaningful results on parenchyma segmentation.

20 thorax-axial CT images are considered to adjust the parameters of framework, and Table 2 is formed in which red results symbolizes the best ones. In Table 2, blue results symbolize the second best results having to a deviation about -0.8% (Jaccard) from the best results. The second best results are utilised to generalize the operation of framework and to fix the parameter values. Because, parameters cannot be fixed in case only the best results are considered.

Table 3 presents the repetition number of all parameter choices, and optimum operation conditions are revealed as the result of 20 different trials. According to Table 3;

- Tolerance value of "50" was efficient on all trials, and can be regarded as the optimum tolerance.
- Once size of structuring element is assigned as "4", optimum results were achieved by means of five statistical metrics on 18/20 trials. Concerning this, optimum size of element can be assigned as "4".
- The optimum duality of $[h_s, h_r]$ is [40,32] at which the best results were achieved on all trials.
- The Lupsix output ensued the optimum results when $M = 0.2$ or $M = 0.3$ on all trials. However, the optimum threshold was "0.3" since the best results of this choice were more than the choice of "0.2".

Table 2. Optimum parameter values obtained on training dataset

| Image | Tolerance of RG | Size of Structuring Element | [h _v ,h _r] | Threshold in MSS |
|-----------|-------------------|-----------------------------|---|---|
| Train_001 | 30,40,50,20 | 3,2,4,5 | [48,24],[32,32],[40,40],[24,32],[24,40],[24,48],[32,24],[32,40],[32,48],[40,24],[40,32],[40,48],[48,16],[48,32],[48,40] | 1,1.5,2,0.1,0.2,0.3,0.4,0.5,0.6,0.7,0.8,0.9 |
| Train_002 | 40,30,50,60 | 4,3,5,6 | [48,16],[24,24],[32,32],[40,40],[32,16],[32,24],[40,16],[40,24],[40,32],[48,24],[48,32],[48,40] | 0.3,0.1,0.2,0.4,0.5,0.6,0.7,0.8,0.9,1 |
| Train_003 | 50,30,40,60 | 4,2,3,5,6 | [32,40],[32,32],[40,40],[16,40],[16,48],[24,40],[24,48],[32,48],[40,32],[48,24],[48,32],[48,40] | 0.4,0.5,0.6,0.1,0.2,0.3,0.7,0.8,0.9,1,1.5,2 |
| Train_004 | 50,30,40 | 3,2,4 | [32,40],[24,24],[32,32],[40,40],[24,16],[24,32],[24,40],[24,48],[32,16],[32,24],[32,48],[40,16],[40,24],[40,32],[48,16],[48,24],[48,32],[48,40] | 0.1,0.3,0.4,0.2,0.5,0.6,0.7,0.8,0.9,1,1.5,2 |
| Train_005 | 60,30,40,50,70 | 2,3,4,5,6 | [24,40],[16,16],[24,24],[32,32],[40,40],[16,24],[16,32],[16,40],[16,48],[24,8],[24,16],[24,32],[24,48],[32,8],[32,16],[32,24],[32,40],[40,8],[40,16],[40,24],[40,32],[48,8],[48,16],[48,24],[48,32],[48,40] | 0.1,0.2,0.3,0.4,0.5,0.6,0.7,0.8,0.9,1,1.5,2 |
| Train_006 | 40,30,50 | 2,3,4,5 | [40,40],[32,32],[16,48],[40,32] | 0.8,0.9,1,0.2,0.3,0.4,0.5,0.6,0.7,1.5 |
| Train_007 | 60, 50 | 4, 3 | [32,32],[40,40],[32,24],[40,24],[40,32] | 0.3,0.1,0.2,0.4,0.5,0.6,0.7,0.8,0.9 |
| Train_008 | 50,30,40,60,70 | 3,2,4 | [48,40],[32,32],[40,40],[48,48],[16,32],[16,40],[16,48],[24,32],[24,40],[24,48],[32,40],[32,48],[40,32],[40,48],[48,32] | 0.1,0.2,0.3,0.4,0.5,0.6,0.7,0.8,0.9,1 |
| Train_009 | 40,20,30,50 | 6,2,3,4,5 | [40,32],[8,8],[16,16],[24,24],[32,32],[40,40],[16,24],[16,32],[16,40],[16,48],[24,8],[24,16],[24,32],[24,40],[24,48],[32,8],[32,16],[32,24],[32,40],[40,8],[40,16],[40,24],[48,8],[48,16],[48,24],[48,32] | 2,0.1,0.2,0.3,0.4,0.5,0.6,0.7,0.8,0.9,1,1.5 |
| Train_010 | 70,20,30,40,50,60 | 3,2,4,5,6 | [32,48],[40,40],[48,48],[24,48],[32,40],[40,32],[40,48],[48,40] | 0.5,0.6,0.7,0.1,0.2,0.3,0.4,0.8,0.9,1,1.5,2 |
| Train_011 | 70,30,40,50,60 | 2 | [48,40],[40,40],[32,40],[32,48],[40,24],[40,32],[48,24],[48,32] | 0.4,0.1,0.2,0.3,0.5,0.6,0.7,0.8,0.9,1,1.5 |
| Train_012 | 40,20,30,50 | 2,3,4,5 | [48,16],[16,16],[24,24],[32,32],[16,8],[16,24],[16,32],[24,8],[24,16],[24,32],[32,8],[32,16],[32,24],[40,8],[40,16],[40,24],[40,32],[48,8],[48,24],[48,32] | 0.1,0.2,0.3,0.4,0.5,0.6,0.7,0.8,0.9,1,1.5,2 |
| Train_013 | 70,20,30,40,50,60 | 4,2,3,5 | [48,48],[24,24],[32,32],[40,40],[24,32],[24,40],[32,16],[32,24],[32,40],[40,16],[40,24],[40,32],[48,16],[48,24],[48,32],[48,40] | 0.3,0.2 |
| Train_014 | 40,20,30,50,60 | 3,2,4,5 | [48,32],[16,16],[24,24],[32,32],[40,40],[16,24],[16,32],[16,40],[16,48],[24,16],[24,32],[24,40],[24,48],[32,16],[32,24],[32,40],[32,48],[40,16],[40,24],[40,32],[48,16],[48,24],[48,40] | 0.1,0.2,0.3,0.4,0.5,0.6,0.7,0.8,0.9,1,1.5,2 |
| Train_015 | 20,30,40,50,60,70 | 3,2,4 | [40,40],[32,32],[24,32],[32,40],[40,32],[40,48],[48,32],[48,40] | 0.3,0.1,0.2,0.4,0.5,0.6,0.7,0.8,0.9,1,1.5 |
| Train_016 | 70,20,30,40,50,60 | 2 | [40,48],[24,24],[32,32],[40,40],[48,48],[16,32],[16,40],[16,48],[24,32],[24,40],[24,48],[32,24],[32,40],[32,48],[40,16],[40,24],[40,32],[48,24],[48,32],[48,40] | 0.2,0.1,0.3,0.4,0.5,0.6,0.7,0.8,0.9,1,1.5,2 |
| Train_017 | 40,30,50 | 2,3,4 | [32,24],[32,32],[24,32],[32,40],[40,24],[40,32],[48,24],[48,32] | 0.1,0.2,0.3,0.4,0.5,0.6,0.7,0.8,0.9,1 |
| Train_018 | 30,40,50 | 4,2,3,5,6 | [40,40],[16,40],[16,48],[24,48],[32,40],[32,48],[40,24],[40,32],[48,24],[48,32],[48,40] | 0.3,0.1,0.2,0.4,0.5,0.6,0.7,0.8,0.9,1,1.5,2 |
| Train_019 | 50, 40 | 4, 5 | [24,32],[32,32],[40,40],[24,40],[32,24],[32,40],[40,32] | 0.3,0.1,0.2,0.4,0.5,0.6,0.7,0.8,0.9,1,1.5 |
| Train_020 | 60,30,40,50 | 3,2,4,5,6 | [32,32],[24,24],[40,40],[24,16],[24,32],[24,40],[24,48],[32,16],[32,24],[32,40],[32,48],[40,16],[40,24],[40,32],[40,48],[48,16],[48,24],[48,32],[48,40] | 0.4,0.5,0.6,0.7,0.8,0.9,1,1.5,0.1,0.2,0.3,2 |

3.2. Experimental Results and Analysis

For an objective and challenging comparison, we have used 20 CT images on training, while data number is chosen as 150 on test. Besides, we control whether every operator of system is necessary or not. Table 4 shows the results with / without operators of Lupsix on a randomly chosen CT image.

According to Table 4, every operator upgrades the performance of system, and the best performance cannot be achieved without these operators as seen in the gaps between with / without results. RG algorithm play a selector role on the choice of lung regions and concerning this, it's not included as a section in Table 4.

Table 3. Repetition number of parameter values

| Parameter Name | Parameter Value | Repetition Number among All Trials (20 Training Images) |
|------------------------------------|-----------------|---|
| Tolerance | 10 | 0 |
| | 20 | 8 |
| | 30 | 18 |
| | 40 | 19 |
| | 50 | 20 |
| | 60 | 12 |
| | 70 | 7 |
| Size of Structuring Element | 2 | 17 |
| | 3 | 17 |
| | 4 | 18 |
| | 5 | 13 |
| | 6 | 7 |
| | [8,8] | 1 |
| | [16,16] | 4 |
| [hs,hr] | [24,24] | 9 |
| | [32,32] | 17 |
| | [40,40] | 18 |
| | [48,48] | 4 |
| | [16,8] | 1 |
| | [16,24] | 4 |
| | [16,32] | 6 |
| | [16,40] | 7 |
| | [16,48] | 8 |
| | [24,8] | 3 |
| | [24,16] | 6 |
| | [24,32] | 13 |
| | [24,40] | 11 |
| | [24,48] | 11 |
| | [32,8] | 3 |
| | [32,16] | 8 |
| | [32,24] | 13 |
| | [32,40] | 16 |
| | [32,48] | 10 |
| | [40,8] | 3 |
| | [40,16] | 9 |
| | [40,24] | 14 |
| | [40,32] | 20 |
| [40,48] | 6 | |
| [48,8] | 3 | |
| [48,16] | 9 | |
| [48,24] | 14 | |
| [48,32] | 16 | |
| [48,40] | 14 | |
| Threshold | 0.1 | 18 |
| | 0.2 | 20 |
| | 0.3 | 20 |
| | 0.4 | 19 |
| | 0.5 | 19 |
| | 0.6 | 19 |
| | 0.7 | 19 |
| | 0.8 | 19 |
| | 0.9 | 19 |
| | 1 | 18 |
| 1,5 | 15 | |
| 2 | 11 | |

Training and test results are presented in Table 5. According to Table 5, Lupsix achieves to better sensitivity, specificity, DSC and Jaccard rates on test dataset meaning that parameter settings of framework were obtained as optimal, and Lupsix can perform the task of segmentation on new images (test dataset) with more

reliable performance.

Table 4. Performance evaluation of Lupsix operators

| <i>Performance Without Sections (With / Without)</i> | Accuracy | DSC | Jaccard |
|--|----------------------|----------------------|----------------------|
| GC | 99.63 / 16.13 | 98.85 / 27.77 | 97.73 / 16.13 |
| MC | 99.63 / 99.55 | 98.85 / 98.59 | 97.73 / 97.21 |
| CLAHE | 99.63 / 37.20 | 98.85 / 33.93 | 97.73 / 20.43 |
| MSS | 99.63 / 16.13 | 98.85 / 27.77 | 97.73 / 16.13 |
| The Filling Process | 99.63 / 99.51 | 98.85 / 98.46 | 97.73 / 96.97 |

Table 5. Performance evaluation of Lupsix on datasets

| Dataset | Sensitivity | Specificity | Accuracy | DSC | Jaccard |
|---------|--------------|--------------|--------------|--------------|--------------|
| Train | 97,91 | 99,67 | 99,33 | 98,17 | 96,41 |
| Test | 98,07 | 99,72 | 99,30 | 98,59 | 97,23 |

3.3. Visual Results and Interpretations

Figure 2 shows the visual results of Lupsix for different conditions. As seen in Figure 2;

- Lupsix operators can effectively divide the parenchyma tissue from other tissues in thorax CT image,
- Lupsix can work on different shaped and sized parenchyma tissues by achieving high segmentation performance,
- Lupsix segments different parenchyma tissues having various grey levels. At this point, proposed framework can perform the segmentation on both homogenous and heterogeneous tissues,
- Lupsix is not effected from the deformations stated in lung parenchyma,
- As a result, an efficient framework is designed to be utilized before disease determination and classification, tumor segmentation and specification, nodule detection, vessel segmentation and abnormality categorization.

Table 6 presents the comparison of Lupsix with the state-of-the-art techniques on lung segmentation. According to the results, it's seen that DSC rate of Lupsix remain promising among other studies in the literature, and the best accuracy is achieved by proposed system. Consequently, a robust segmentation system is presented to the literature for segmentation of lung parenchyma.

Table 6. The literature comparison on lung segmentation

| Study | Techniques | Accuracy | Dice |
|---------------------|---|----------|--------|
| Wei et al. [9] | System based on improved chain code and Bresenham algorithm | 95.2% | ---- |
| Dai et al. [10] | Pipeline involving graph cuts, Gaussian mixture models (GMMs) and expectation maximization (EM) | ---- | 98.74% |
| Noor et al. [11] | Framework including thresholding and morphology based segmentation coupled with feedback | ---- | 98.4% |
| Pulagam et al. [12] | The modified convex hull approach and morphological operators | ---- | 98.62% |
| Chae et al. [13] | MLevel-set | 98.4% | ---- |
| Zhang et al. [14] | Hybrid geometric active contour model | ---- | 97.7% |
| This study | Lupsix | 99.3% | 98.59% |



Fig. 2. Outputs of Lupsix operators

4. Conclusions

In this paper, lung parenchyma segmentation is handled, and an efficient & semi-automated framework is designed to obtain the parenchyma in thorax-axial CT images.

For this purpose, Lupsix is formed by using histogram analysis, morphological approaches, MSS and RG algorithms to efficiently segment the parenchyma. As a result, a robust framework is achieved challenging to the state-of-the-art techniques in the literature.

According to the experiments, it's seen that Lupsix segmented the lung parenchyma with higher success rates on test data than training dataset. Also we kept the training data (20 images) very low according to the test data (150 images) so as to perform an objective and challenging comparison. On the other hand, a detailed examination is performed to find the optimum operation conditions of Lupsix. Concerning this, high segmentation performance is achieved by the combinatory work of necessary operators in Lupsix.

In future work, Lupsix will be utilized as the segmentation part of a classification framework in which disease classification will be realized using the parenchyma tissue obtained as the output of Lupsix.

References

- [1] S. Zhou, Y. Cheng, and S. Tamura, "Automated lung segmentation and smoothing techniques for inclusion of juxtapleural nodules and pulmonary vessels on chest CT images," *Biomed. Signal Process.*, vol. 13, pp. 62-70, 2014.
- [2] S. Shen, A. A. Bui, J. Cong, and W. Hsu, "An automated lung segmentation approach using bidirectional chain codes to improve nodule detection accuracy," *Comput. Biol. Med.*, vol. 57, pp. 139-149, 2015.
- [3] M. Obert, M. Kampschulte, R. Limburg, S. Barańczuk, and G. A. Krombach, "Quantitative computed tomography applied to interstitial lung diseases," *Eur. J. Radiol.*, 2018.
- [4] M. Z. Ur Rehman, M. Javaid, S. I. A. Shah, S. O. Gilani, M. Jamil, and S. I. Butt, "An appraisal of nodules detection techniques for lung cancer in CT images," *Biomed. Signal Process.*, vol. 41, pp. 140-151, 2018.
- [5] A. Mansoor, U. Bagci, B. Foster, Z. Xu, G. Z. Papadakis, L. R. Folio, J. K. Udupa, and D. J. Mollura, "Segmentation and image analysis of abnormal lungs at CT: current approaches, challenges, and future trends," *RadioGraphics*, vol 35, no. 4, pp. 1056-1076, 2015.
- [6] B. A. Skourt, A. El Hassani, and A. Majda, "Lung CT Image Segmentation Using Deep Neural Networks," *Procedia Comput. Sci.*, vol. 127, pp. 109-113, 2018.

- [7] X. Liao, J. Zhao, C. Jiao, L. Lei, Y. Qiang, and Q. Cui, "A segmentation method for lung parenchyma image sequences based on superpixels and a self-generating neural forest," *Plos One*, vol. 11, no. 8, e0160556, 2016.
- [8] T. Doel, D. J. Gavaghan, and V. Grau, "Review of automatic pulmonary lobe segmentation methods from CT," *Comput. Med. Imag. Grap.*, vol. 40, pp. 13-29, 2015.
- [9] Y. Wei, G. Shen, and J. J. Li, "A fully automatic method for lung parenchyma segmentation and repairing," *J. Digit. Imaging*, vol. 26, no.3, pp. 483-495, 2013.
- [10] S. Dai, K. Lu, J. Dong, Y. Zhang, and Y. Chen, "A novel approach of lung segmentation on chest CT images using graph cuts," *Neurocomputing*, vol. 168, pp. 799-807, 2015.
- [11] N. M. Noor, J. C. Than, O. M. Rijal, R. M. Kassim, A. Yunus, A. A. Zeki, M. Anzidei, L. Saba, and J. S. Suri, "Automatic lung segmentation using control feedback system: morphology and texture paradigm," *J. Med. Syst.*, vol. 39, no.3, 22, 2015.
- [12] A. R. Pulagam, G. B. Kande, V. K. R. Ede, and R. B. Inampudi, "Automated lung segmentation from HRCT scans with diffuse parenchymal lung diseases," *J. Digit. Imaging*, vol. 29, no.4, pp. 507-519, 2016.
- [13] S. H. Chae, H. M. Moon, Y. Chung, J. Shin, and S. B. Pan, "Automatic lung segmentation for large-scale medical image management," *Multimed. Tools Appl.*, vol. 75, no.23, pp. 15347-15363, 2016.
- [14] W. Zhang, X. Wang, P. Zhang, and J. Chen, "Global optimal hybrid geometric active contour for automated lung segmentation on CT images," *Comput. Biol. Med.*, vol. 91, pp. 168-180, 2017.
- [15] S. Armato III, G. McLennan, L. Bidaut, M. McNitt-Gray, C. Meyer, A. Reeves, and L. Clarke, "Data from LIDC-IDRI," *The cancer imaging archive*, 2015
- [16] S. G. Armato *et al.*, "The lung image database consortium (LIDC) and image database resource initiative (IDRI): a completed reference database of lung nodules on CT scans," *Med. Phys.*, vol. 38, no.2, pp. 915-931, 2011.
- [17] K. Clark *et al.*, "The Cancer Imaging Archive (TCIA): maintaining and operating a public information repository," *J. Digit. Imaging*, vol. 26, no. 6, pp. 1045-1057, 2013.
- [18] P. Charles, "Digital Video and HDTV Algorithms and Interfaces," Morgan Kaufmann Publishers, San Francisco, 2003.
- [19] R. C. Gonzalez, R. E. Woods, S. L. Eddins, "Digital image processing using MATLAB," McGraw Hill Education, New York, 2009.
- [20] H. Koyuncu, R. Ceylan, M. Sivri, H. Erdogan, "An Efficient Pipeline for Abdomen Segmentation in CT Images," *J. Digit. Imaging*, vol. 31, no.2, pp. 262-274, 2018.
- [21] K. Zuiderveld, "Contrast limited adaptive histogram equalization," in: *Graphics gems IV*, P. S. Heckbert, Ed. San Diego, CA, USA: Academic Press Professional Inc., 1994, pp. 474-485.
- [22] P. Soille, "Morphological Image Analysis: Principles and Applications," Springer-Verlag, 1999, pp. 173-174.
- [23] D. Comaniciu, P. Meer, "Mean shift: A robust approach toward feature space analysis," *IEEE T. Pattern Anal.*, vol. 24, no. 5, pp. 603-619, 2002.
- [24] H. Koyuncu, R. Ceylan, H. Erdogan, M. Sivri, "A novel pipeline for adrenal tumour segmentation," *Comput. Meth. Prog. Bio.*, vol. 159, pp. 77-86, 2018.
- [25] S. W. Franklin, S. E. Rajan, "Computerized screening of diabetic retinopathy employing blood vessel segmentation in retinal images," *Biocybern. Biomed. Eng.*, vol. 34, pp. 117-124, 2014.